First-principles study of HgTe/CdTe heterostructures under perturbations preserving time-reversal symmetry

Jonas Anversa and Paulo Piquini*
Departamento de Fisica, Universidade Federal de Santa Maria, 97105-900, Santa Maria, RS, Brazil

Adalberto Fazzio
Instituto de Fisica, Universidade de São Paulo, CP 66318, 05315-970, São Paulo, SP, Brazil

Tome M. Schmidt
Instituto de Fisica, Universidade Federal de Uberlândia, CP 593, 38400-902, Uberlândia, MG, Brazil
(Received 26 April 2014; revised manuscript received 5 October 2014; published 21 November 2014)

The observation of the quantum spin Hall effect without the need of an external magnetic field in HgTe/CdTe heterostructures triggered the study of materials exhibiting persistent spin-polarized electronic currents at their interfaces. These Dirac-like spin states are predicted to be topologically protected against perturbations preserving time-reversal symmetry. However, nonmagnetic (time-reversal preserving) perturbations will certainly affect these interface states. In this work, the density functional theory is used to characterize the topologically protected states of the (001) HgTe/CdTe heterostructure as well as to understand the influence of external adiabatic parameters as pressure and electric fields on these states. The intrasite Hubbard U term is seen to be important to correctly describe the HgTe bulk band structure. It is shown that, differently from the three-dimensional topological insulators, the HgTe/CdTe interface states present fully in-plane Rashba-like spin texture. Further, biaxial external pressures and electric fields perpendicular to the interfaces are seen to change the energetics and dispersion of the protected states, modifying the energy ordering of the crossing of the polarized interface states inside the band structure, and altering their Fermi velocities while not changing the topological quantum phase. These adiabatic variables can then be used to tune the topologically protected states with respect to the Fermi level.

DOI: 10.1103/PhysRevB.90.195311 PACS number(s): 73.20.−r, 73.21.Fg

I. INTRODUCTION

The topological insulators (TIs) constitute a material phase with potential application in spintronics and quantum information [1], serving also as a platform to investigate fundamental physics concepts [2]. This new field in solid-state physics is based on the fact that the spin-orbit interaction can turn a material with a fully insulating gap in the bulk into one presenting gapless surface/interface states, which are protected against perturbations preserving time reversal symmetry (TRS). This phenomenon, called quantum spin Hall effect (QSHE), was proposed by Kane *et al.* [3]. Bernevig *et al.* [4] showed that a HgTe/CdTe quantum well structure would be a material system where the QSHE could be observed. This was successfully verified by the Molenkamps group [5], through electronic transport measurements, showing for the first time the distinctive signature of the interface spin-polarized states on this class of topological insulator (TI) materials.

After this decisive experimental verification, several theoretical and experimental studies have been performed aiming to find new TI materials, and to understand the underlying physical principles governing the QSHE [6,7]. In a recent work, Küfner and Bechstedt [8] used *ab initio* density functional theory to study the edge states of HgTe quantum wells and qualitatively verified the previous result of a four-band $\mathbf{k}\cdot\mathbf{p}$ approach [4]. On the other hand, Luo and Zunger [9], using an atomistic pseudopotential method, showed that the topological states of the HgTe/CdTe heterostructure are two-dimensional (2D) interface states, instead of 1D edge states as proposed by Bernevig *et al.* [4]. Fu and Kane [10] introduced a method to evaluate the Z_2 invariants, and used a four-band tight-binding model to obtain these invariants in 2D and 3D TIs. Most of the transport properties of the HgTe/CdTe quantum well have been intensively studied [11,12]. The effects of transverse electric fields on HgTe/CdTe heterostructures have been studied by Liu *et al.* [13]. Chen *et al.* [14] studied the influence of a magnetic field on electronic transport in HgTe/CdTe quantum wells and showed that the quantum spin Hall effect can survive under magnetic fields up to 10 T. Wang *et al.* [15] obtained that the transport through the QSH state is robust, with the conductivity having a constant value of $2e^2/h$ independently of the number, shape, strength, or length of the scattering potential. Sengupta *et al.* [16] used the $\mathbf{k}\cdot\mathbf{p}$ method to study the critical well thickness dependence on external stress, temperature, and electric fields.

However, the effective application of future devices based on TI materials requires an accurate characterization of the gapless topological states as well as an understanding of how these states behave under usual external perturbations. Hence, an accurate description of the band structure of TIs through density functional theory calculations under different external conditions is crucial. In this work we show that a correct description of the levels close to the top of the valence band of the HgTe band structure requires the inclusion of the intrasite Hubbard U Coulomb repulsion term in the density functional formalism. The evolution of the band structure of

*paulo.piquini@ufsm.br

the HgTe/CdTe as a function of the barrier (CdTe) and well (HgTe) thicknesses is investigated. Differently from the 3D TIs, the spin texture of the Dirac-like states is seen to be fully in the interface plane. Further, focusing on real applications using 2D topological insulators, we study the effects of external adiabatic parameters, in order to define any phase transition, as well as to understand how the protected topological states react under different perturbations. Our results demonstrate that external pressure and electric field affect the band structure of HgTe/CdTe heterostructure. They can be used to tune the energetic position of the topologically protected states.

II. METHODOLOGY

The density functional theory is used to study the HgTe and CdTe bulk materials as well as the HgTe/CdTe heterostructures. The exchange and correlation contributions are evaluated using the PW91 functional [17]. The interaction between the ionic cores and valence electrons is described by the projected augmented wave approach [18]. All total energy calculations explicitly consider the spin-orbit interaction. A Γ-centered Monkhorst-Pack scheme [19] is used to generate a k-point mesh in the reciprocal space in order to obtain a total energy convergence within 5 meV. This convergence is obtained using a $6 \times 6 \times 6$ mesh for the bulk materials, and a $10 \times 10 \times 1$ mesh for the heterostructures. The Kohn-Sham single-particle wave functions are represented by plane-wave expansions with a cutoff of 280 eV.

The optimization of the zinc-blende HgTe and CdTe bulk lattice constants lead to 6.65 and 6.63 Å, respectively. These values are in good agreement with the experimental ones [20], which are 6.45 and 6.48 Å for HgTe and CdTe, respectively, but in a reverse order. This could lead to stresses at the HgTe/CdTe interfaces that are reverse to that actually observed. Due to this fact, we choose to use the average lattice constants for the bulk materials, 6.465 Å, in the studied HgTe/CdTe heterostructures.

For the cases where the heterostructure is subjected to biaxial pressures, i.e., for pressures at the interface plane, the out-of-plane lattice constant is changed in order to keep constant the total volume of the supercell (isochoric process). On the other hand, for the cases where an external electric field is applied perpendicularly to the interface plane, the HgTe well is connected to 10 CdTe layers at each side. These CdTe layers are truncated, their dangling bonds are saturated with H atoms, and a vacuum layer of 12 Å is kept between neighboring supercells along the direction perpendicular to the interface plane. For all the studied cases full atomic relaxations are performed, except when an electric field is applied, where the outmost CdTe layers are kept fixed.

III. RESULTS AND DISCUSSIONS

A. Electronic structure of HgTe and CdTe bulk materials

In order to verify the accuracy of our theoretical approach as well as to establish a standard that can reproduce the important characteristic features of the studied systems, calculations have been performed for the HgTe and CdTe bulk materials. The band structure for the zinc-blende CdTe and HgTe bulk materials are shown in Fig. 1. The band gap of CdTe is around 0.49 eV, which is in agreement with previous *ab initio* calculations [21,22] but is lower than the experimentally observed value, 1.60 eV [20]. The HgTe band structure correctly shows a metallic behavior. However, the energetic ordering of the Γ_6 (s-like electron-level centered on the Hg atom) and Γ_7 (p-like split-off level) levels are inverted, with the Γ_7 appearing higher in energy than Γ_6. The correct description of the Γ_6/Γ_7 energetic ordering is crucial to study the topologically protected surface/interface states appearing at the interface between the HgTe bulk and trivial insulators. In order to correct the energetic ordering between the Γ_6 and Γ_7 levels we used the GGA+U approach. We used a value of 9.4 eV for the intrasite effective Hubbard U term (actually $U - J$ [23], with $J = 1$ eV), on the $5d$ level of Hg. This was determined by requiring not only that the Γ_6 level be higher in energy than Γ_7 (which could be achieved with a $U = 2.4$ eV) but also to match the experimental results [24], see Table I. This approach leads to the band structure shown in Fig. 1(c), where a change at the Γ point for the first level below the top of the valence band is clearly seen. The characterization of the levels below the Fermi energy is made through a spd decomposition of the Bloch bulk levels into spherical harmonics at spheres centered on each ion.

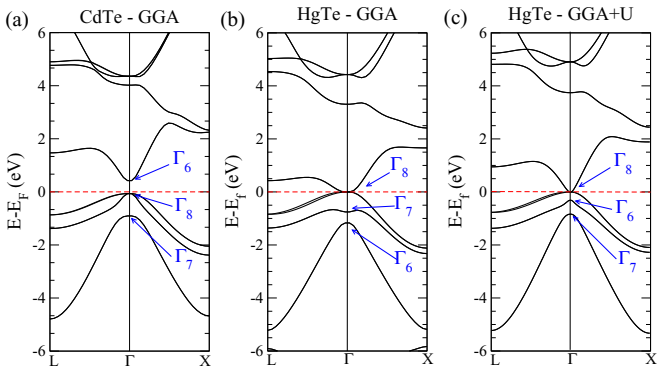

FIG. 1. (Color online) Band structures for the zinc-blende (a) CdTe, and (b) HgTe bulk materials with DFT/GGA approach. In (c) the band structure for the zinc-blende HgTe bulk material calculated using the DFT/GGA+U approach, with $U - J = 9.4$ eV on the Hg $5d$ level.

The changes in the band structure due to the inclusion of the intrasite Hubbard U term occur due to the p-d repulsion. The changes in the s, p, and d projected density of states of the HgTe bulk material are shown in Fig. 2, with the d-like

TABLE I. The energy band gap, $E_g = \Gamma_6 - \Gamma_8$, and the spin-orbit splitting, $\Delta_{so} = \Gamma_8 - \Gamma_7$, for the HgTe bulk material. Negative values for E_g mean an inverted order between the Γ_8 and Γ_6 levels.

	GGA	GGA+U	theory	expt.[a]
E_g	−1.14	−0.31	−0.27[b], −0.60[c], −0.34[d]	−0.29
Δ_{so}	0.87	0.84	0.89[b], 0.91[c], 0.78[d]	0.91

[a]From Ref. [24].
[b]From Ref. [25].
[c]From Ref. [26].
[d]From Ref. [27].

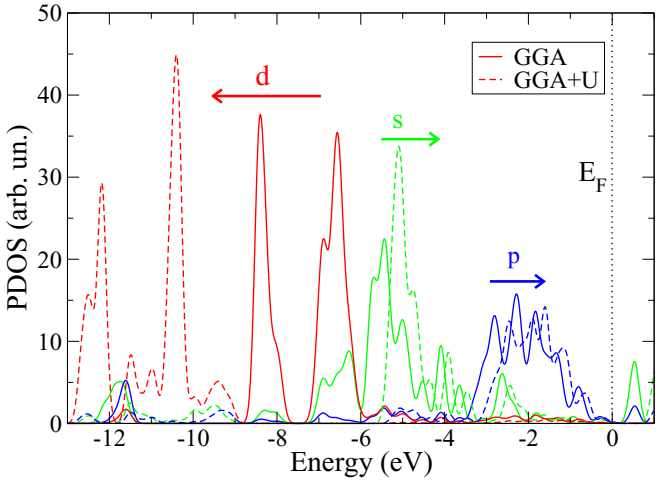

FIG. 2. (Color online) Calculated projected density of states (PDOS) for the HgTe bulk using GGA (solid line) and GGA+U (dotted line) DFT approaches.

levels going deeper into the valence band, and the s- and p-like levels moving toward the top of the valence band.

B. Electronic structure of [001] HgTe/CdTe heterostructures

We begin our study of the (001) HgTe/CdTe heterostructures by verifying the thickness of the CdTe layer that is necessary for the HgTe/CdTe heterostructure to change from a superlattice to a multiple quantum well behavior. This is made varying the CdTe layer thickness while keeping the HgTe layer width fixed to ten unit cells (64.65 Å) along the (001) direction. Once determined the CdTe layer thickness for a multiple quantum well behavior, we fixed it and studied the evolution of the electronic structure of the HgTe/CdTe heterostructure as a function of the HgTe width. This is done in order to analyze the transition from a trivial (at narrow HgTe layer) to a topological insulator (for larger HgTe layers), and also to determine the minimum HgTe well thickness to invert the band gap.

1. *Varying the* HgTe *and* CdTe *thickness*

The band structure of the (001) HgTe/CdTe heterostructure suffers some changes as compared to the HgTe and CdTe individual materials. Topological interface states have been observed on these heterostructures when the HgTe thickness is greater than 63 Å, for a thick CdTe barrier [5], but HgTe and CdTe bulk are not topological materials.

The band structure evolution for varying CdTe barrier thickness and fixed (64.65 Å) HgTe well is shown in Fig. 3. As can be seen in this figure, the band gap, calculated as the energy difference between the (Γ_6 derived) s-like level (red in Fig. 3) and the bottom of the conduction band, is inverted for all considered barrier thickness, showing that 64.65 Å of HgTe is enough for the system to behave as a topological system. The position of s-like level in the band structure (shown as a thick red line segment around the Γ point in Fig. 3) is deep inside the VB for narrow barrier thickness, getting into the top of VB for a CdTe barrier larger than 60 Å. From a comparison between the band structures for barrier thickness of 64.65 Å and 77.58 Å in Fig. 3, it can be seen that the transition from a superlattice to a multiple quantum well behavior is already signaled, since the levels' dispersions do not change significantly when the barrier thickness is increased.

Once we determined the minimum CdTe barrier thickness for a multiple quantum well behavior, we checked the HgTe well thickness necessary to the transition from a trivial to a topological insulator behavior of the interface states in the (001) HgTe/CdTe heterostructure. The band structures for different HgTe thicknesses are shown in Fig. 4, where the s-like level at the Γ point appears as a thick red line. For well thickness thinner than 50 Å, the system clearly behaves as a trivial insulator, with the s-like level at the bottom of the CB, presenting a well-defined energy gap, as shown in Table II. When the well thickness is close to 50 Å both the conduction band minimum and the valence band maximum show a hybridized sp composition, establishing a transition point from a trivial to a topological insulator behavior. For a well thickness equal to 64.65 Å, the HgTe/CdTe heterostructure is already at the topological insulator regime. The calculated transition between the trivial to a topological behavior occurs for a well thickness comparable to that of the experimentally observed

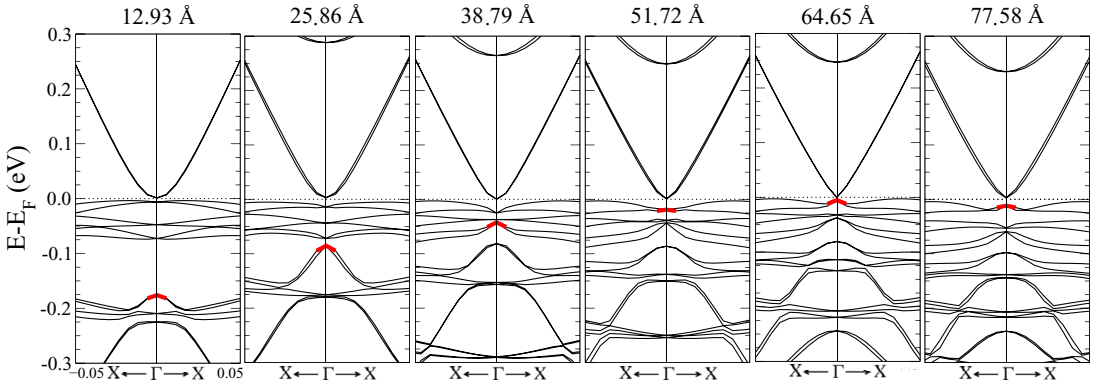

FIG. 3. (Color online) Calculated band structure around Γ point for HgTe/CdTe heterostructure with fixed HgTe thickness (64.65 Å), and variable CdTe thickness. The value of the CdTe thickness appears at the top of each band structure. The red line segments show levels for which the major contributions have a Γ_6 s-like character.

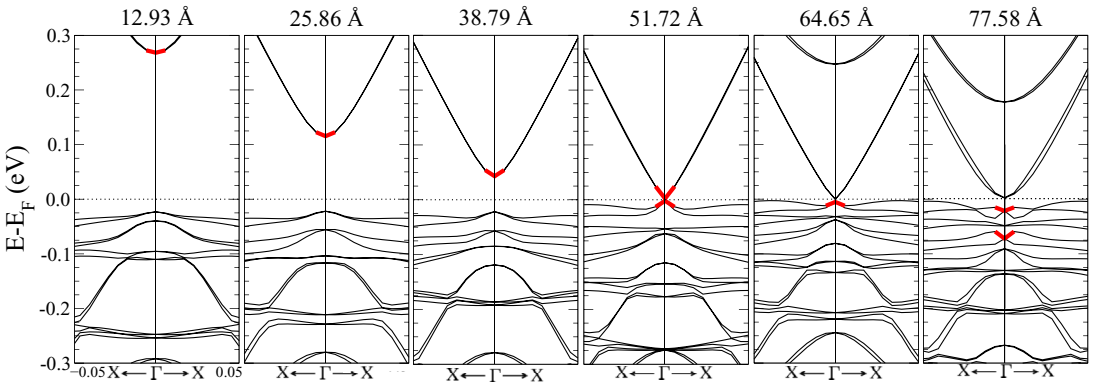

FIG. 4. (Color online) Calculated band structure around Γ point for HgTe/CdTe heterostructure with fixed CdTe thickness (64.65 Å), and variable HgTe thickness. The value of the HgTe thickness appears at the top of each band structure. The red line segments show levels for which the major contributions have a Γ_6 s-like character.

(63 Å). For a well thickness of 77.58 Å, see Fig. 4, it is verified that the band structure of the heterostructure is very similar to that obtained by Luo and Zunger [9], who used a well thickness around 96 Å.

2. *Characterizing the interface states*

In order to characterize the protected interface states we keep the thickness for both barrier (CdTe) and well (HgTe) as 64.65 Å, and look for the interface states that should present the expected planar spin textures. Since the TRS is preserved, a pair of Dirac-like topologically protected interface states (TIS) must lie at each interface.

In Fig. 5 we show the energy band dispersions along the Γ-X [Figs. 5(a) and 5(b)] and Γ-M [Fig. 5(c)] directions of the planar Brillouin zone [Fig. 5(d)] of the CdTe/HgTe interface. We compute the spin polarization components $\langle \mathbf{S}_{n,\alpha}(\mathbf{k})\rangle = (\hbar/2)\langle\phi_n(\mathbf{k})|\sigma_\alpha|\phi_n(\mathbf{k})\rangle$ for a given energy band n, where σ_α are the Pauli matrices for each spin component $\alpha = x, y, z$, and $\phi_n(\mathbf{k})$ are the Kohn-Sham eigenfunctions. The green and red circles for some bands n and k vectors of the band structures shown at Fig. 5 represent the levels with resulting up and down spin polarizations, respectively, along the CdTe/HgTe interface direction. The size of circles are directly related to the magnitude of the spin polarization. The black dots appearing in the band structures designate the levels whose charge densities have major contributions coming from the interface layers. As can be seen from the band structures at Fig. 5, some levels located at the interfaces have net spin polarization, while others have no spin polarization. The Dirac-like TIS must satisfy both conditions: (i) be located at the interfaces, and (ii) have net spin polarizations. This distinction between interface states with and without spin polarization in the band structures of the HgTe/CdTe heterostructure is important to the correct identification of the TIS. As is clearly shown in the results at Fig. 5, there are highly localized interface states close to the top of the valence band (heavy holes) that are not spin polarized. These states should not be recognized as contributing to the TIS.

TABLE II. Eigenvalue difference between the s-like level and the p-like level for varying (a) CdTe barrier, and (b) HgTe well thickness.

	E_g	
	(a)	(b)
12.93	− 0.18	0.29
25.86	− 0.09	0.14
38.79	− 0.04	0.06
51.72	− 0.02	0.003
64.65	− 0.005	− 0.005
77.58	− 0.012	− 0.022

As can be seen from Fig. 5, the helical Dirac pair states present opposite spin components, as it should be. More interestingly, the spin polarization of the Dirac states is completely in plane, showing no component at directions perpendicular to the interface. We have computed the spin-projected density of states (SPDOS), defined as $P_\alpha(E) = \sum_{n,\mathbf{k}}\langle S_{n,\alpha}(\mathbf{k})\rangle\delta(E - E_n(\mathbf{k}))$, using only one side of the band structures along $\Gamma \rightarrow X$ and $\Gamma \rightarrow M$ directions, see the right panels of Figs. 5(a)–5(c). For the $\Gamma \rightarrow X$ direction we observe that $P_x(E) = P_z(E) = 0$. The SPDOS computed along the k_x direction (not shown here) presents only $P_y(E)$ as nonzero projection. For the $\Gamma \rightarrow M$ direction, the $P_x(E)$ and $P_y(E)$ are nonzero, with $P_z(E) = 0$. These results show that the helical spin texture of the Dirac states is fully in plane, differently from the 3D TI materials Bi_2Se_3 and Bi_2Te_3, where there is always some out-of-plane spin component [28,29]. This scenario is compatible with the spin texture induced by the Rashba effect, as shown by Ganishev *et al.* [30]. This is in contrast with previous investigations [9], which suggested that the spin splitting would appear due to a Dresselhaus effect.

In order to fully characterize the spin texture of the Dirac-like TIS states, we have computed the spin-resolved energy contour of the TIS states for three energy windows, two below and one above the Fermi energy, as shown in Fig. 6. The results on Fig. 6 emphasize the helical structure of the spin texture of the TIS states.

We have estimated the total spin polarizations at each interface by summing up the spin polarizations for interface states whose eigenvalues are within the range of 0.1 eV (below and above) of the Fermi energy. The ratio between the calculated total spin polarizations between the two interfaces is around 3, showing an asymmetry that could be, in principle, experimentally verified.

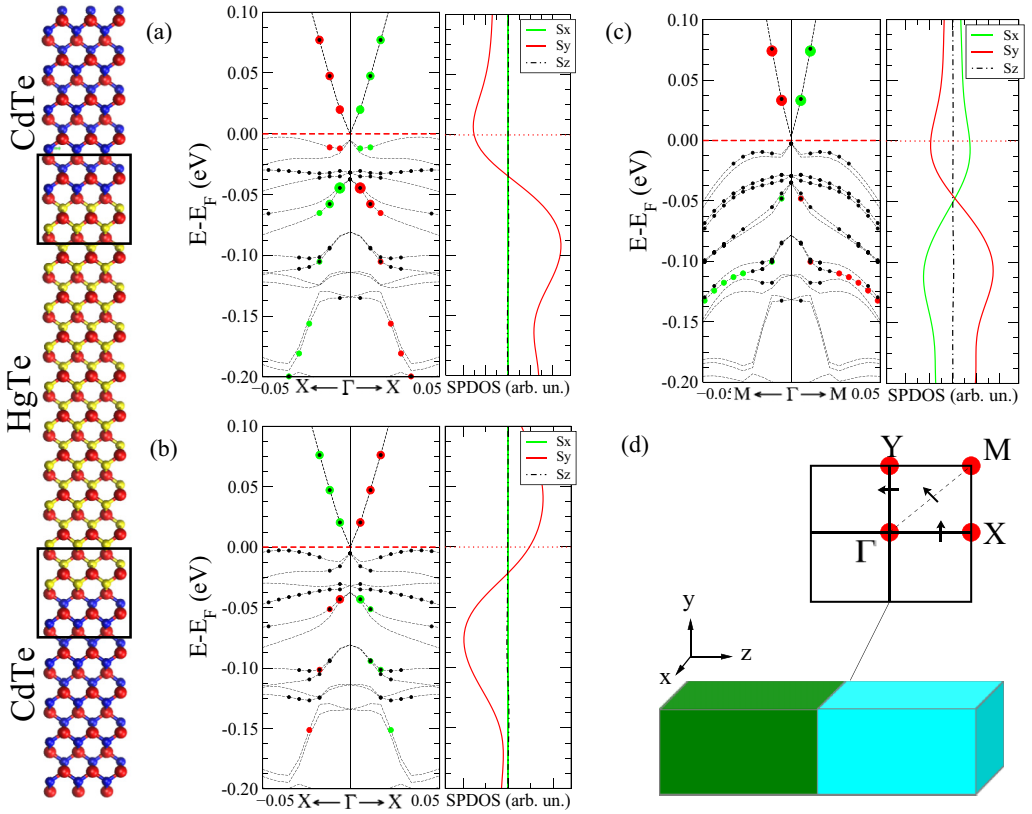

FIG. 5. (Color online) The figure at the left side illustrates the unit cell of the HgTe/CdTe heterostructure. The middle panel shows the calculated band structures for the $\Gamma \rightarrow X$ direction of the planar Brillouin zone and their respective spin textures (S_x, S_y, and S_z) for half the band structure for (a) the interface at the top, and (b) the interface at the bottom of the illustrative picture. The right panel shows in (c) the band structure and spin textures of the top interface for the $\Gamma \rightarrow M$ direction, and in (d) a schematic representation of the spin configuration at the planar Brillouin zone. The green and red points represent the levels with resulting spin-up and spin-down polarizations, respectively. The points in black designate the states whose charge densities are concentrated at the interface regions, i.e., the interface states. The spin textures were calculated by considering the layers inside the black boxes of the illustrative picture.

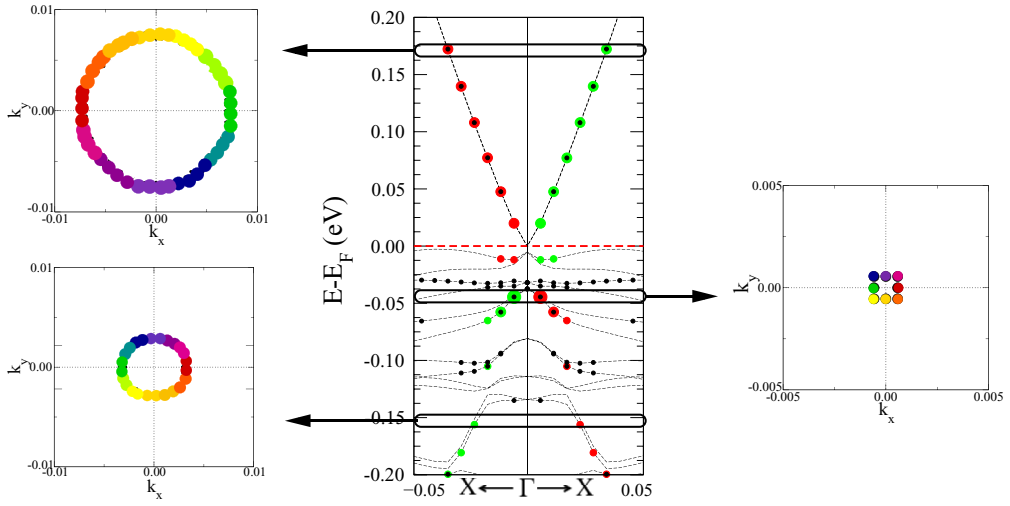

FIG. 6. (Color online) The calculated spin-resolved energy contours for three selected spin-polarized interface states, one above and two below TIS crossing point. The green, red, violet, and gold colors represent the $S_y \uparrow$, $S_y \downarrow$, $S_x \uparrow$, and $S_x \downarrow$, respectively. The intermediate colors mean that the direction of the spin polarization is gradually changing between its values on the coordinate axes.

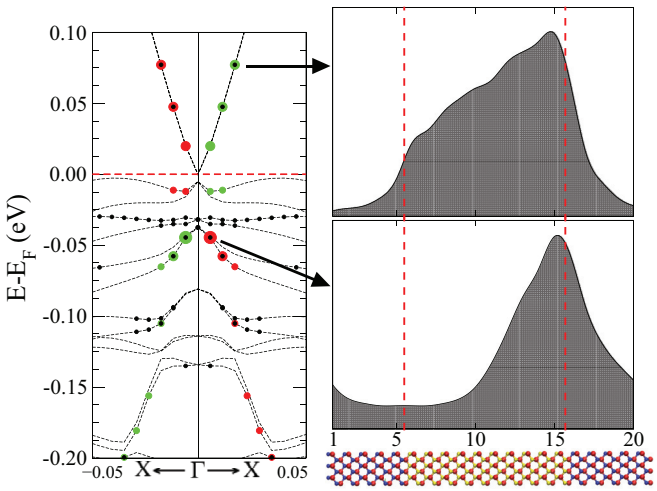

FIG. 7. (Color online) The right panel shows the calculated charge densities of specific levels along the heterostructure HgTe/CdTe. The picture below the charge densities represents the HgTe/CdTe heterostructure unit cell (the colors follow the same pattern of Fig. 5), and allows one to identify the charge density values with the different regions of the heterostructure. The arrows coming from the HgTe/CdTe band structure indicate which levels are being considered to the charge density analysis. The green and red circles represent the levels with resulting up and down spin polarization, respectively. The size of the circles are directly related to the magnitude of the spin polarization. The points in black designate the states whose charge densities are concentrated at the interface regions, i.e., the interface states.

From the SPDOS shown in Fig. 5 we observe that the Dirac crossing (the energy where the SPDOS change the sign) is not exactly at the Fermi energy, but it is below it, close to the top of the valence band.

It is important to spatially characterize the Dirac-like TIS. We observe that TIS comes mostly from the interfaces, but there is some contribution also from the well. A general feature from the TIS levels is that the closest the level is to the Γ point the greater the contributions from the interface region. This can be seen in Fig. 7, where the charge densities from two specific levels along the band corresponding to the TIS are shown. The level closest to the Γ point is clearly concentrated at the interface, while the level a little farther from the Γ point show contributions coming from the inner part of the HgTe well, while keeping the peak at the interface. This shows that the levels composing the TIS band have a variable spatial distribution, being concentrated at the interface, while turning more delocalized inside the HgTe well when the representative k point moves away from the Γ point.

C. HgTe/CdTe heterostructures under external pressures

In order to better characterize the TIS and to understand the degree of protection, especially for real device applications, it is important to verify how the TIS behave under perturbations that preserve TRS. Our results show that external pressures do not destroy the protected interface states, but do induce some characteristic changes in the energetic position and dispersion of the TIS, as can be seen in Figs. 8 and 9.

For hydrostatic tensile stress (+1% and +2% of a_0), the crossing of the TIS levels appears deeper inside the bulk valence band. On the other hand, for compressive stress (−1% and −2% in Fig. 8) the crossing remains almost at the same energetic position relatively to the Fermi energy. Actually, the crossing moves in energy in a way that closely follows the highest energy levels of the valence band at the Γ point, showing that the action of hydrostatic pressures on HgTe/CdTe heterostructures are not capable to markedly distinguish the TIS levels from the bulk levels.

For external biaxial pressures, on the other hand, a different behavior is observed. From Fig. 9 one can see that the effect from biaxial stress on the Dirac-like interface states is completely distinct from the other bulk valence states. For tensile strains the TIS crossing goes up, while for compressive strains it goes down inside the bulk valence band, not showing a direct connection with the behavior of the remaining bulk valence levels.

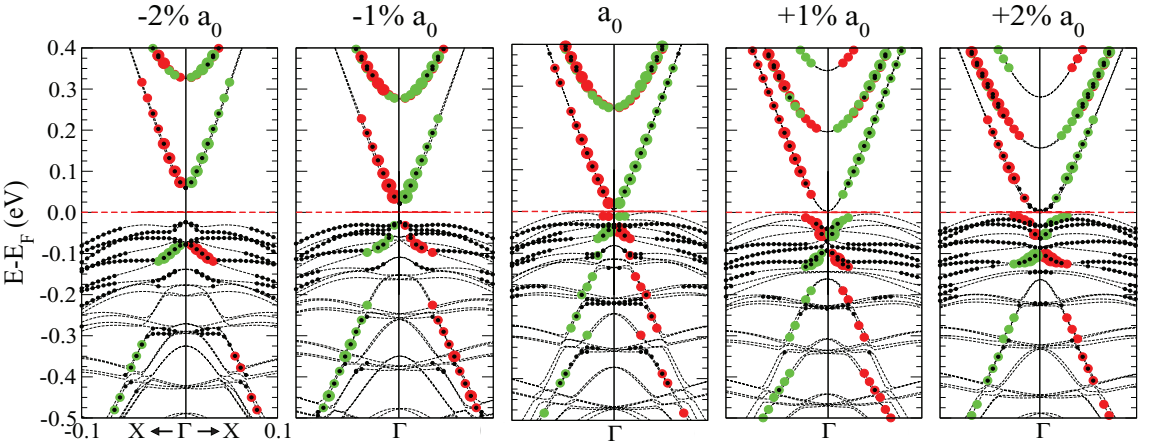

FIG. 8. (Color online) Calculated band structures for one interface of the HgTe/CdTe heterostructures subjected to external hydrostatic pressures. The values on top of each band structure represent the variation of the lattice constant relatively to the stress free configuration. Positive (negative) percentage values result in tensile (compressive) stress, respectively. The green and red circles represent the levels with resulting up and down spin polarization, respectively. The size of the circles are directly related to the magnitude of the spin polarization. The points in black designate the states whose charge densities are concentrated at the interface regions, i.e., the interface states.

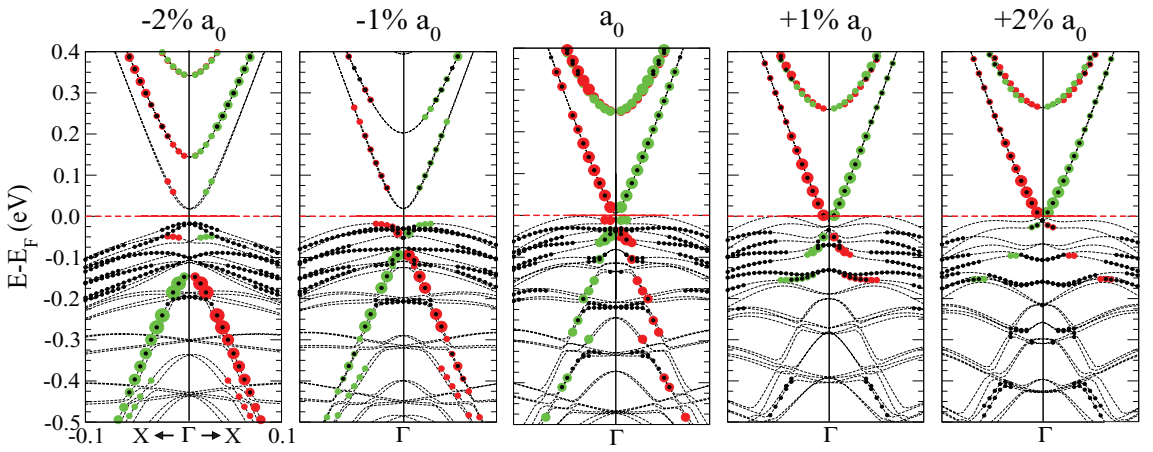

FIG. 9. (Color online) Calculated band structures for one interface of the HgTe/CdTe heterostructures subjected to external biaxial pressures. The values on top of each band structure represent the variation of the lattice constant relatively to the stress free configuration. Positive (negative) percentage values result in tensile (compressive) stress, respectively. The green and red circles represent the levels with resulting up and down spin polarization, respectively. The size of the circles are directly related to the magnitude of the spin polarization. The points in black designate the states whose charge densities are concentrated at the interface regions, i.e., the interface states.

One interesting feature observed for biaxial external pressures is the variation of the magnitude of spin polarization between the segments of the TIS levels appearing below and above the crossing point. We estimated these magnitudes by the value of the total spin polarization of the TIS states closest to the crossing point. Table III shows the results for all the studied cases (including the hydrostatic pressures). As can be seen from this table, in the equilibrium situation (no external stress), the spin polarization for the levels below and above the crossing point have the same value. When biaxial tensile (compressive) stresses are applied, there is an increase in the magnitude of spin polarization for the levels above (below) the crossing point. For hydrostatic pressures no specific tendencies are observed.

For both kinds of external pressures, hydrostatic and biaxial, a gap opening is observed for compressive stresses. More importantly, an increasing parabolicity of the TIS levels is observed for increasing external pressures. This means that the TIS levels will gradually lose its Dirac-like dispersion with increasing external pressures, which will consequently change the Fermi velocities.

D. HgTe/CdTe heterostructures under external electric field

External electric fields can be used to change quantum phase transition as well as work as a gate for device applications. Electric fields can turn 3D or 2D topologically nontrivial insulators into trivial ones and vice versa [31–33].

TABLE III. Percentage of the spin polarization before and after the crossing for the hydrostatic and biaxial pressures.

	Hydrostatic					Biaxial				
	−2%	−1%	0%	+1%	+2%	−2%	−1%	0%	+1%	+2%
Before	0.2	0.2	0.25	0.25	0.25	0.2	0.2	0.25	0.25	0.3
After	0.2	0.25	0.25	0.25	0.25	0.3	0.25	0.25	0.2	0.2

By applying electric fields perpendicular to the HgTe/CdTe interface, as shown in Fig. 10, we observe that the TIS crossing at one interface goes down, while in the other interface it goes up. This asymmetry of the TIS crossings is due to the difference on the electrostatic potential at each interface. We have calculated the average electrostatic potential along the (001) direction for the cases of no external electric field, and for an external electric field of 5×10^{-3} eV/Å, as shown in Fig. 11. From this figure one can note that the electric dipoles at the interfaces point to opposite directions, which explains the opposite energetic displacements of the TIS levels at each interface. Further, even for the zero-field case, there is a difference between the magnitude of the interface electric dipoles, which could explain the already discussed different total spin polarizations at each interface.

For a HgTe well width around 60 Å, even without an external electric field, we observe that the TIS are not degenerate in energy, which means that the TIS at the neighboring interfaces interact. The interaction between the external electric field and the interface dipoles will enhance this asymmetry, as clearly seen at right columns of Fig. 10.

As the TIS crossing is always close in energy to some bulk bands, it is hard to determine if there is a gap opening by looking the band structure by applying the external electric field. However by focusing on the spin texture, we clearly can see that there is no gap opening for electric fields up to 5×10^{-3}V/Å. A gap opening should be expected if the two interfaces interact with each other, or by breaking TRS. We do not see any gap for the electric field and the well width presented in this calculation. So a phase transition from topological to trivial insulator is only expected for larger electric fields or due to the presence of defects, which could break TRS, which is absent here.

One aspect of the TIS that becomes more evident with the application of an external electric field is the Rashba splitting of the levels with opposite spin polarizations. This appears clearly for the states at the bottom of the conduction for electric fields of 2×10^{-3} and 5×10^{-3} eV/Å, see Fig. 10.

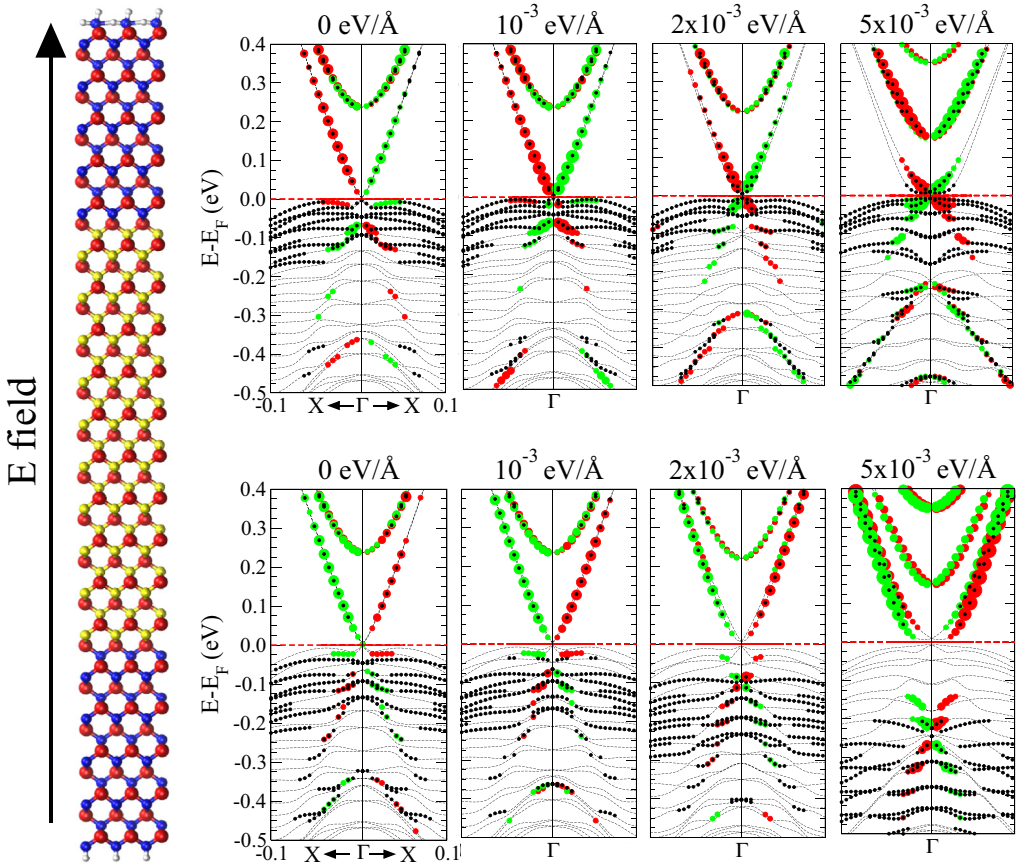

FIG. 10. (Color online) The picture at the right side illustrates the CdTe/HgTe/CdTe quantum well unit cell and the direction of the applied electric field. Also shown are the calculated band structures for the interfaces at (a) the top, and (b) the bottom part of the quantum well. The values of the applied external electric fields appear on top of each band structure. The green and red circles represent the levels with resulting up and down spin polarization, respectively. The size of the circles are directly related to the magnitude of the spin polarization. The points in black designate the states whose charge densities are concentrated at the interface regions, i.e., the interface states.

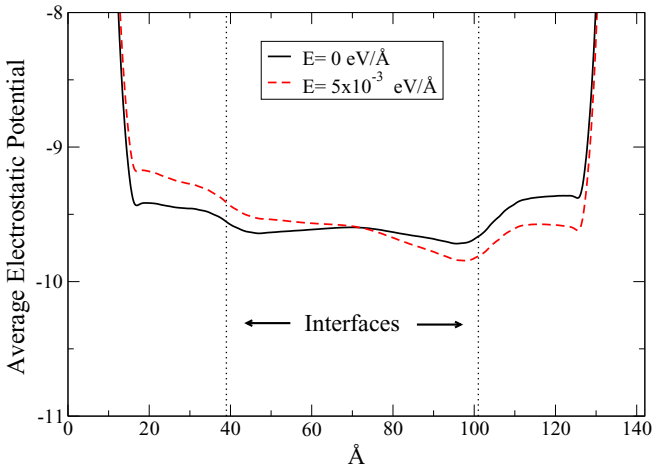

FIG. 11. (Color online) The calculated average electrostatic potential, $\overline{V}_{el}$, along the direction perpendicular to the interface planes of the (001) HgTe/CdTe heterostructure. The solid black line shows the $\overline{V}_{el}$ without external electric field, while the dashed red line shows the $\overline{V}_{el}$ for an applied external electric field of 5×10^{-3} eV/Å. The vertical dotted lines show the position of the interfaces.

It should be noted here that in contrast to the effects of biaxial stress, which move the TIS levels of both interfaces in the same direction, the effect of external electric fields perpendicular to the heterostructure interface depends on the direction of the interface dipoles, leading to opposite effects on the TIS of (001) HgTe/CdTe heterostructures with D2*h* symmetry.

IV. CONCLUSIONS

To describe the HgTe band structure within density functional formalism an intrasite Coulomb U repulsion must be explicitly included. Using this approach we characterize the topologically protected states of HgTe/CdTe heterostructure. The gapless protected states, which are only present for HgTe well width greater than 60 Å, present Rashba-like spin texture fully in plane. There is no out-of-plane spin component as has been observed in 3D topological insulators. We show that a correct understanding of the TIS depends crucially on the distinction between interfaces states with and without spin polarization. Our results show that the TIS crossing is located bellow the top of the valence band, but it can be

moved by adiabatic external parameters that do not change the topological quantum phase of the HgTe/CdTe heterostructure. Biaxial external pressures and electric fields perpendicular to the interface will directly influence the electronic structure of the HgTe/CdTe heterostructures, making them useful tools to tune the protected topological state position. Further, we observe that external pressure can affect the Fermi velocity. This understanding of how the topological states can be manipulated by perturbations preserving time-reversal symmetry is certainly very important for the design and operation of devices using topological insulators.

ACKNOWLEDGMENTS

We acknowledge the financial support from the Brazilian Agencies CNPq, CAPES, FAPESP, and FAPEMIG. The calculations have been performed using the computational facilities of CENAPAD/Campinas.

[1] L. Zhao, J. Liu, P. Tang, and W. Duanb, Appl. Phys. Lett. **100**, 131602 (2012).
[2] N. Nagaosa, Science **318**, 758 (2007).
[3] C. L. Kane and E. J. Mele, Phys. Rev. Lett. **95**, 146802 (2005).
[4] B. A. Bernevig, T. L. Hughes, and S.-C. Zhang, Science **314**, 1757 (2006).
[5] M. König, S. Wiedmann, C. Brüne, A. Roth, H. Buhmann, L. W. Molenkamp, X.-L. Qi, and S.-C. Zhang, Science **318**, 766 (2007).
[6] M. Z. Hazan and C. L. Kane, Rev. Mod. Phys. **82**, 3045 (2010).
[7] X.-L. Qi and S.-C. Zhang, Rev. Mod. Phys. **83**, 1057 (2011).
[8] S. Küfner and F. Bechstedt, Phys. Rev. B **89**, 195312 (2014).
[9] J.-W. Luo and A. Zunger, Phys. Rev. Lett. **105**, 176805 (2010).
[10] L. Fu and C. L. Kane, Phys. Rev. B **76**, 045302 (2007).
[11] C. Brüne, C. X. Liu, E. G. Novik, E. M. Hankiewicz, H. Buhmann, Y. L. Chen, X. L. Qi, Z. X. Shen, S. C. Zhang, and L. W. Molenkamp, Phys. Rev. Lett. **106**, 126803 (2011).
[12] D. G. Rothe, E. M. Hankiewicz, B. Trauzettel, and M. Guigou, Phys. Rev. B **86**, 165434 (2012).
[13] G. Liu, G. Zhou, and Y.-H. Chen, Appl. Phys. Lett. **99**, 222111 (2011).
[14] J. C. Chen, J. Wang, and Q.-F. Sun, Phys. Rev. B **85**, 125401 (2012).
[15] Y.-X. Wang and S.-J. Xiong, Mod. Phys. Lett. B **25**, 2001 (2011).
[16] P. Sengupta, T. Kubis, Y. Tan, M. Povolotskyi, and G. Klimeck, J. Appl. Phys. **114**, 043702 (2013).
[17] J. P. Perdew, J. A. Chevary, S. H. Vosko, K. A. Jackson, M. R. Pederson, D. J. Singh, and C. Fiolhais, Phys. Rev. B **46**, 6671 (1992).
[18] P. E. Blöchl, Phys. Rev. B **50**, 17953 (1994).
[19] H. J. Monkhorst and J. D. Pack, Phys. Rev. B **13**, 5188 (1976).
[20] Landolt-Börnstein, *in Semiconductors, Physics of Group IV Elements and III-V Compounds*, edited by O. Madelung, M. Schulz, and H. Weiss, New Series, Group III, Vol. 17 (Springer-Verlag, New York, 1982).
[21] J. Heyd, J. E. Peralta, G. E. Scuseria, and R. L. Martin, J. Chem. Phys. **123**, 174101 (2005).
[22] S.-H. Wei, S. B. Zhang, and A. Zunger, J. Appl. Phys. **87**, 1304 (2000).
[23] V. I. Anisimov, J. Zaanen, and O. K. Andersen, Phys. Rev. B **44**, 943 (1991).
[24] N. Orlowski, J. Augustin, Z. Golacki, C. Janowitz, and R. Manzke, Phys. Rev. B **61**, R5058 (2000).
[25] J. W. Nicklas and J. W. Wilkins, Phys. Rev. B **84**, 121308 (2011).
[26] R. Sakuma, C. Friedrich, T. Miyake, S. Blügel, and F. Aryasetiawan, Phys. Rev. B **84**, 085144 (2011).
[27] A. Svane, N. E. Christensen, M. Cardona, A. N. Chantis, M. van Schilfgaarde, and T. Kotani, Phys. Rev. B **84**, 205205 (2011).
[28] T. M. Schmidt, R. H. Miwa, and A. Fazzio, Phys. Rev. B **84**, 245418 (2011).
[29] O. V. Yazyev, J. E. Moore, and S. G. Louie, Phys. Rev. Lett. **105**, 266806 (2010).
[30] S. D. Ganichev, V. V. Bel'kov, L. E. Golub, E. L. Ivchenko, P. Schneider, S. Giglberger, J. Eroms, J. De Boeck, G. Borghs, W. Wegscheider, D. Weiss, and W. Prettl, Phys. Rev. Lett. **92**, 256601 (2004).
[31] M. Kim, C. H. Kim, H.-S. Kim, and J. Ihm, Proc. Natl. Acad. Sci. **109**, 671 (2011).
[32] J. Li and K. Chang, Appl. Phys. Lett. **95**, 222110 (2009).
[33] T. Zhang, J. Ha, N. Levy, Y. Kuk, and J. Stroscio, Phys. Rev. Lett. **111**, 056803 (2013).